A Caution on the Use of Surface Digital Elevation Models to Simulate Supraglacial Hydrology of the Greenland Ice Sheet

Kang Yang, Laurence C. Smith, Vena W. Chu, Colin J. Gleason, and Manchun Li

***Abstract*—Digital elevation models (DEMs) of ice surface topography are often used for hydrologic analysis of the Greenland ice sheet (GrIS), but their suitability for this purpose has received little quantitative assessment. We compare remotely sensed maps of supraglacial lakes, rivers, and moulins with their DEM-modeled counterparts, using two moderate-resolution DEMs (SPIRIT DEM and ASTER GDEM) for a $\sim$24 000 km^2 area of the southwestern GrIS. We find that modeled hydrological features are critically sensitive to selection of a depression area threshold (a user-specified parameter used to fill noise and/or true topographic depressions in the ice surface DEM), with small depression area thresholds over-predicting observed supraglacial lake abundance and large thresholds under-predicting lake abundance. Few remotely sensed moulins are identified in either DEM, even if a small depression area threshold is used. A standard practice of filling all DEM depressions yields modeled surface flow paths that broadly match remotely sensed supraglacial river networks, but are far less fragmented than reality (owing to moulin capture), raising into question the realism of this standard practice. In sum, moderate-resolution DEMs do hold value for simulating broad-scale hydrography of the GrIS surface, but are critically sensitive to choice of the filling threshold, and insensitive to moulins which also influence supraglacial drainage pattern. Our preliminary analysis suggests using a depression area threshold of $0.1-0.2$ km^2 for lakes, advises against using DEMs to predict moulin locations, and urges caution when using 100% DEM filling to model flow paths of supraglacial rivers.**

***Index Terms*—Digital elevation model (DEM), Greenland ice sheet (GrIS), hydrology, supraglacial lake, supraglacial river.**

I. Introduction

THE Greenland ice sheet (GrIS) has experienced extensive mass loss in recent decades, and surface meltwater runoff and ice discharge are the two main causes [1], [2]. Meltwater runoff losses are large (e.g., 71–256 Gt/yr or 50–84% [3]) and have received growing attention in the last decade. Such estimates are commonly derived from surface mass balance (SMB) modeling [4] and GRACE satellite gravity anomalies [5]. However, neither approach considers surface meltwater routing (i.e., supraglacial rivers), storage (i.e., in supraglacial lakes), or coupling with the englacial system (i.e., moulins) [2]. Therefore, advancing meltwater transport processes in SMB models will require better understanding of supraglacial hydrologic features (lakes, rivers, and moulins), especially if they can be derived from readily available digital elevation models.

The most direct way to identify these features is through satellite mapping. Many studies have mapped lakes on the GrIS via low- or moderate-resolution satellite images, while mapping of supraglacial rivers had not been attempted until recently [6]. For instance, McGrath *et al.* manually delineated supraglacial river networks upstream of a moulin using WorldView-1 panchromatic imagery and assessed the summer water budget in that catchment [7]. Joughin *et al.* digitized a subset of rivers in a small region along Greenland's west coast using WorldView-1/2 and qualitatively revealed the spatial extent of the internal catchments in the region [8]. Lampkin and VanderBerg detected wide supraglacial channels in the Jakobshavn Isbræ region from Landsat-7 panchromatic imagery and analyzed their relationships with lakes [9]. Yang and Smith developed an automated procedure to delineate supraglacial river networks from WorldView-2 multispectral imagery [10]. However, while direct mapping of surface rivers in satellite imagery provides high-quality results, synoptic characterization of supraglacial hydrology is difficult due to variable spectral contrast between meltwater and ice/snow. Moreover, high-resolution images covering the GrIS are still sparsely dispersed spatially and temporally, and only "snapshots" of supraglacial drainage patterns can be expected.

In contrast, digital elevation models (DEMs) are readily available across most parts of the ice sheet, attracting considerable interest for the purpose of modeling supraglacial drainage patterns over large areas of the ice sheet [11]–[14]. These DEMs are generally produced by using stereo remote sensing images (e.g., 10 m SPOT 5, 15 m ASTER, and 0.5 m WorldView-1/2). In addition to their ubiquity, a prime motivation for using DEMs to model supraglacial hydrologic features on the ice sheet is the relative ease by which these features may be derived, using standard GIS tools developed for hydrologic analysis in terrestrial systems [15]. However, many practitioners are not fully aware of the limitations of DEMs for hydrologic analysis, in particular the effect of DEM accuracy

Manuscript received June 08, 2015; revised August 10, 2015; accepted September 24, 2015. This work was supported in part by the National Natural Science Foundation of China under Grant 41501452, in part by the Fundamental Research Funds for the Central Universities under Grant 020914380014, and in part by the NASA Cryosphere Program under Grant NNX14AH93G.

K. Yang and M. Li are with the Department of Geographic Information Science, Nanjing University, Nanjing 210023, China (e-mail: manchunli_geo@126.com).

L. C. Smith and C. J. Gleason are with the Department of Geography, University of California, Los Angeles, CA 90095 USA.

V. W. Chu is with the Department of Geography, University of California, Berkeley, CA 94709 USA.

Color versions of one or more of the figures in this paper are available online at http://ieeexplore.ieee.org.

Digital Object Identifier 10.1109/JSTARS.2015.2483483

on drainage network delineation and topographic depression identification [16]–[18].

Like terrestrial systems, surface meltwater (supraglacial) flow on the ice sheet is controlled primarily by surface topography [19]. Ideally, a common practice is to simply fill all depressions (which are assumed as topography noise [18]), thus forcing all supraglacial drainage networks to have high interconnectivity and flow without interruption all the way to the ice edge [19]. However, in reality, numerous actual topographic depressions exist on the ice surface and host supraglacial lakes or moulins, consequently acting as meltwater sinks and fragmenting supraglacial drainage networks via many internally drained catchments [2], [13], [14], [20]. For example, Arnold *et al.* proposed a supraglacial meltwater routing model and revealed how topographic depressions were filled during summer [13]. Clason *et al.* added lake drainage events into another meltwater routing model and further investigated the supraglacial hydrologic impacts of the topographic depressions [14]. Generally, all the DEM-modeled depressions were considered as potential meltwater sinks in these meltwater routing models. However, these depressions could be either actual topographic characteristics or DEM noise [21], [22]. As such, it is problematic to either keep or fill all of the DEM-modeled depressions. This situation complicates assessments of GrIS DEM suitability for supraglacial hydrologic analysis, because a DEM's ability to indicate the locations of drainage sinks must be analyzed in addition its ability to follow the observed supraglacial drainage network.

Depression area thresholds are commonly used to discern actual depressions from artificial ones. The underlying idea of this thresholding approach is that a certain number of DEM pixels are required to form an actual topographic depression and thus the small ones that fail to pass a user-specified area threshold are considered as noise and should be filled [22]. It is problematic to either keep or fill all the DEM-modeled depressions. The choice of the depressions area thresholds significantly impacts the performance of the DEM-modeled supraglacial hydrologic patterns. As such, particular attention should be dedicated to the choice of depression area thresholds.

This study provides a first assessment of how supraglacial hydrologic drainage characteristics modeled from moderate-resolution ($\sim$30 m) DEMs compare with mapped hydrologic features obtained from multisource satellite imagery. First, DEM-modeled hydrologic features (depressions and drainage networks) were compared with their observed counterparts (supraglacial lakes, moulins, and river networks) to address the following questions. 1) Can DEM-modeled depressions predict the locations of the observed supraglacial lakes and depict the shapes of these lakes correctly? 2) Can DEM-modeled drainage networks reasonably represent the patterns of the observed supraglacial river networks? 3) Can DEM-modeled depressions predict the locations of the observed moulins? Second, we conducted experiments to assess the impact of the selected depression area threshold on the abundance and spatial pattern of predicted surface water features on the ice sheet. Third, because the remotely sensed observations were not simultaneous with DEM acquisition, the stability of supraglacial drainage patterns over time was also considered. Viewed collectively, the study provides useful insight about the benefits and limitations of using moderate-resolution DEMs to model the flow of meltwater passing over and into the ice sheet surface.

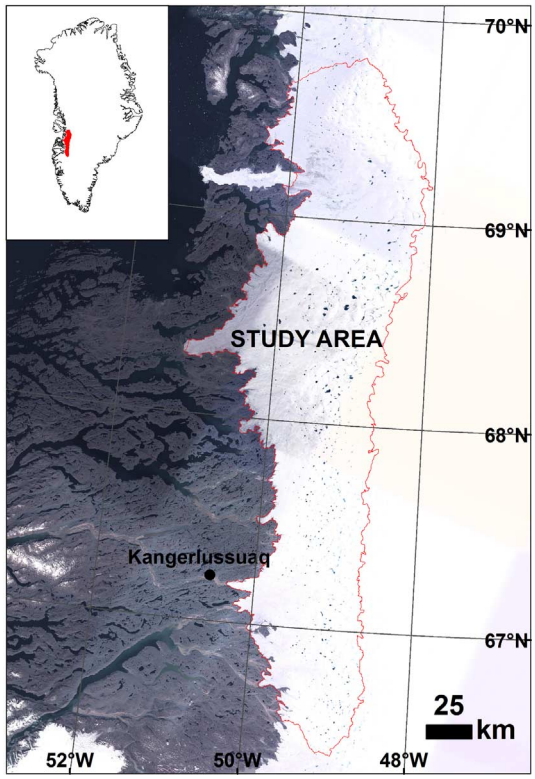

Fig. 1. Landsat TM mosaic map of the study area (red outline) showing numerous supraglacial lakes formed in response to surface melting. The study area is situated along the Greenland ice sheet's southwestern margin. Elevations within this area range from 600 to 1400 m a.s.l. The extent of this study area is from the ice edge (*left*) to the 1400 m contour (*right*), and from the Sermeq Avannarleq glacier (north) to the Sukkertoppen Iskappe glacier (south). This area is known for the largest number of sudden lake drainage events, rapid melt-induced velocity changes, and extensive surface melting of any area studied on the Greenland ice sheet.

II. Study Site

The study area is situated along the Greenland ice sheet's southwestern margin, covering a $\sim$24 000 km^2 area between the Sermeq Avannarleq and the Sukkertoppen Iskappe glaciers (Fig. 1). GrIS elevations within this area range from 600 to 1400 m a.s.l., completely below the mean equilibrium line altitude (ELA) of 1600–1800 m [23]. This area is rich in supraglacial hydrologic features, with numerous supraglacial lake, river, and moulins forming on the ice surface each melt season [24]. It has been subject to several hydrologic modeling studies, revealing a significant and accelerated mass loss owing to increasing surface meltwater runoff in this area [4]. In particular, it is known for the largest number of sudden lake drainage events, rapid melt-induced velocity changes, and extensive surface melting of any area studied on the GrIS.

Numerous topographic depressions are distributed on the ice surface in this area, collecting meltwater and forming supraglacial lakes during melt seasons [13]. This area is also reported to exhibit more supraglacial lakes than any other areas on the GrIS [24]. The formation, evolution, and drainage of the supraglacial lakes in this area have been well studied

using multiresolution satellite imagery [25]–[27]. Supraglacial river networks also develop very well in this area, forming huge and complex surface drainage patterns each summer [9]. These networks are the primary surface meltwater pathways and can transport meltwater to moulins with high efficiency [2]. Moulins typically form at the intersections of supraglacial rivers and crevasses (type I moulins, outside depressions) or on the bottom surface of supraglacial lakes (type II moulins, inside depressions) [2]. It is possible to detect type II moulin occurrences directly by identifying abrupt drainage of corresponding supraglacial lakes, or indirectly by modeling depressions in DEMs [28]. However, identification of type I moulin occurrences using only DEM data is much more difficult: if type I moulins are the dominant type of moulins on the GrIS, DEMs will perform poorly in identifying the locations of moulins and consequently fail to detect the moulin-induced meltwater sinks on the ice sheet.

III. Data and Methods

A. DEM Datasets

The SPIRIT (SPOT 5 stereoscopic survey of Polar Ice: reference images and topographies) and GDEM (global digital elevation model) v2 were used as the ice surface topographic models in this study. The SPIRIT DEM is an International Polar Year (IPY) project and was generated from optical stereo-images obtained by the SPOT-5 satellite over the period 2007–2009. It has a 40-m spatial resolution and a horizontal precision of 30-m RMS, with a demonstrated vertical accuracy of ± 6 m in the vicinity of Jakobshavn Isbrae in the northern portion of our study area [29]. The ASTER GDEM is an elevation dataset with nearly global coverage and is based on a composition of the automatically generated DEMs from ASTER stereo scenes acquired since 2000 [30]. The GDEM data have a spatial resolution of 30 m and a horizontal precision of 30 m RMS, with a demonstrated vertical accuracy of ± 20 m in the southwestern coastal regions of the GrIS [31]. This study used the v2 GDEM, a reprocessed product using an updated algorithm and incorporating additional ASTER images acquired after 2008, thus improving both vertical and horizontal accuracies. The GDEM data were obtained from the USGS LPDAAC (http://lpdaac.usg.gov). Finally, the SPIRIT DEM data were resampled to 30 m to facilitate comparisons with the GDEM data. The primary reason that we up-sampled SPIRIT DEM instead of down-sampling GDEM is to follow the procedures proposed in [32] and facilitate consistent DEM analyses and applications in the field. In addition, the performance of 30-m SPIRIT DEMs is very similar to that of the original 40 m products based on several experimental tests. Furthermore, we focused on mono scale (30 m) analysis in this study and did not analyze the impacts of DEM spatial resolutions on hydrologic modeling [16], [22].

B. Remotely Sensed Datasets

ASTER Level 1A surface reflectance and Landsat-7 ETM+ SLC-on images collected between May 31 and August 23 between 2000 and 2011 were used to extract supraglacial lakes. 81 ASTER and 9 Landsat-7 ETM+ images were acquired from the USGS GLOVIS (http://glovis.usgs.gov/). The spatial resolution of the ASTER images in the visible and near-infrared (NIR) bands is 15 m, and the multispectral Landsat-7 ETM+ images have a spatial resolution of 30 m. The orthorectified horizontal accuracies of ASTER and Landsat-7 ETM+ images were reported to be better than 50 m [33]. An additional precision geolocation was not performed.

Multispectral WorldView-2 (WV2) images acquired from the DigitalGlobe Inc. through the Polar Geospatial Center (www.pgc.umn.edu) were used to delineate surface rivers. WV2 offers a high spatial resolution of ~ 2 m, which is able to depict the supraglacial river networks in great detail [7], [8], [10]. Three multispectral WorldView-2 catalogs (including 21 images) acquired in July 2012 (a period of extensive melting across the entire GrIS [34]) were used in this study These images are located over the southwestern GrIS ablation zone near Kangerlussuaq, covering an area of 3516 km^2. The images were ortho-rectified based on the satellite-positioning model (also known as the Rational Function Model) and projected into a polar stereographic coordinate system using the code developed by the Polar Geospatial Center (https://github.com/PolarGeospatialCenter/imagery_utils).

C. Supraglacial Lake and River Mapping

To enhance detection of supraglacial meltwater in the ASTER, Landsat-7 ETM+, and WV2 visible / near-infrared (NIR) satellite images, a band ratio approach was used. In this study, the ratio of ASTER Band 1 (green, 520–600 nm) and Band 3 (NIR, 760–860 nm), Landsat-7 ETM+ Band 1 (blue, 450–515 nm) and Band 4 (NIR, 775–900 nm), and WV2 Band 2 (blue, 450–510 nm) and Band 8 (NIR, 860–1040 nm) were determined to best enhance supraglacial water on the ice sheet. These band ratio images were used as initial input for lake and river delineation as follows. Atmospheric correction was not conducted because it did not impact water detection.

A simple global and local classification approach was used to delineate supraglacial lakes [35]. First, a normalized global threshold (0.30 for ASTER images and 0.50 for Landsat-7 ETM+ images) was set to classify the band ratio images into open water and ice/snow and obtain initial lake boundaries. These initial boundaries contained numerous inaccuracies due to heterogeneous water spectral characteristics among the images, so further refinement was required. To this end, each initial lake boundary was expanded to generate a buffered lake-background region that was twice the size of the initial lake area. In this buffered region, both snow/ice (background) and lakes have similar areas (pixels), and thus the resultant histogram of the band ratio values in this buffered region was bimodal. Next, the OTSU method was used to classify these buffered regions into open water and image background [36]. The OTSU method searches for the optimal threshold (t) that maximizes the interclass variance in each buffered lake region: $\sigma^2(t) = \omega_1(t)\omega_2(t)[\mu_1(t) - \mu_2(t)]^2$, where σ^2 is the interclass variance, ω_i is the class probability and μ_i is the class mean. Both ω_i and μ_i were calculated from the histogram of the buffered lake region. Thus, an adaptive local threshold (t) was automatically obtained for each lake region, yielding better lake detection results. The boundaries derived from these local

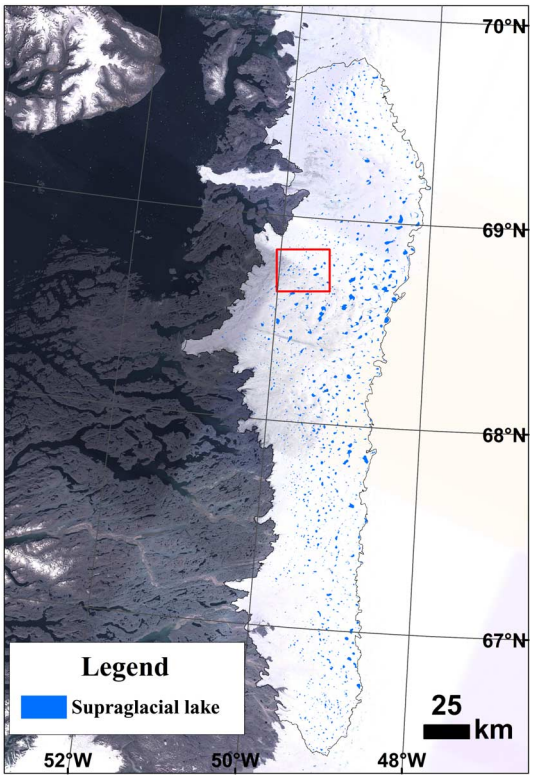

Fig. 2. Maximum supraglacial lake extent, as observed over the period May 31, 2000–August 23, 2010, from 81 ASTER and 9 Landsat-7 ETM+ images. The maximum observed lake extents are derived as a subset of 62 images (54 ASTER images and 8 Landsat-7 ETM+ images), implying a dynamic and complex meltwater filling process over space and time, as different lakes are at their maximum extents at many different times. The red box shows the example region of Fig. 6.

thresholds (0.22–0.35 for ASTER and 0.33–0.60 for Landsat-7 ETM+) were retained as the final lake delineation product for each satellite image (81 ASTER, 9 Landsat-7 ETM+ images). As a final step, the largest such delineations recorded across all images were aggregated to provide a single map of maximum lake extent (Fig. 2). Although ice flows on the GrIS surface, supraglacial lakes are hosted by surface topographic depressions and the formation of these depressions is mainly controlled by bedrock topography so the locations of these depressions/lakes are stable, facilitating maximum lake identification [37]. This maximum observed lake extent map was derived from 62 different images (54 ASTER images and 8 Landsat-7 ETM+ images), implying a dynamic and complex meltwater filling process over space and time as different lakes were at their maximum extents at many different times. In summary, 2311 supraglacial lakes were delineated with areas ranging from 0.004 to 8.7 km^2 and an average area of 0.3 ± 0.7 km^2. The maximum summed area of the supraglacial lakes was 710.0 km^2, covering 3.0% of the study area, lower than the conventionally reported 5.0% [38].

Supraglacial rivers and moulins were a subset of the WV2 ice surface feature map in [2]. In total, 393 supraglacial river networks were delineated with a total length of 4534 km and an average length of 11.5 ± 25.3 km per river network. Most of the supraglacial lakes were drained in those WV2 images so lake–river relationships were not analyzed [9]. All these river networks terminated at a moulin or moulin complex, and finally 424 moulins were visually identified as the ends of these river networks. This revealed a strong link between supraglacial and en-/subglacial meltwater transport and implied an efficient ice surface hydrologic system to drain surface meltwater into the ice sheet.

D. Modeling and Filling Topographic Depressions

A first step in conventional terrestrial DEM-based hydrologic modeling is to fill depressions, also called pits or sinks. A basic assumption in this processing step is that most of the depressions found in DEM data are noise and/or artifacts, and can thus safely be filled (i.e., removed [21] or eliminated [22]) to ensure longitudinal connectivity of drainage flow paths [39]. However, this idealized assumption is clearly not appropriate for the GrIS, where numerous actual topographic depressions are distributed on the ice sheet surface.

To analyze the impact of DEM depressions on the supraglacial drainage pattern, first, all depressions were filled in ArcGIS software to create a depressionless DEM raster. Second, this depressionless raster was subtracted from the original DEM to capture both true and artificial (noise) depressions. Third, different depression area thresholds (A_{dep}) were applied to discern actual depressions from artificial ones (keeping the depressions that passed A_{dep}, while filling the others that failed) and a very small area threshold of $A_{dep} = 0.01$ km^2 ($\sim$10 pixels in the 30 m DEM data) was initially used to assess the raw accuracy of the two tested DEMs. Other possible filling thresholds, e.g., depression depth, slope, or area-depth ratio, were all found to be very noisy and not useful. Finally, those DEM-modeled depressions under different A_{dep} values were compared with satellite-observed supraglacial lakes, quantitatively revealing the abilities of the two DEMs to appropriately reproduce lakes.

E. Comparison of DEM-Modeled Depressions With Remotely Sensed Supraglacial Lakes

Supraglacial lakes must be found in topographic depressions. Hence, satellite-derived supraglacial lakes should represent actual topographic depressions on the ice sheet. If the DEMs are accurate, depressions derived from these models will match well with the locations of satellite-mapped lakes. More specifically, each DEM depression should contain one or more supraglacial lake(s), and each supraglacial lake should lie within one DEM depression.

In reality, perfect match between DEM depressions and remotely sensed lake rarely occurred, owing primarily to accuracy limitations of the DEM data, and classification errors from the satellite data, as well as any temporal changes that transpired between the time of DEM capture and satellite observation. Therefore, a geospatial comparison between depression and lake locations yielded three outcomes as follows (Fig. 3).

1) An observed lake with no DEM depression, signifying that the DEM failed to capture a true topographic low on the ice sheet. This case may be explained by either insufficient DEM accuracy, or because the depressions were

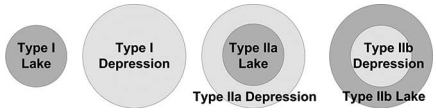

Fig. 3. Schematic representation of the classification of topographic depressions and supraglacial lakes. A "type I" lake is a remotely sensed lake with no corresponding DEM depression, signifying that the DEM data fail to capture a true topographic depression on the ice sheet. A "type I" depression is a DEM depression with no corresponding remotely sensed lake, signifying either DEM noise or moulin development. A spatially coincident depression and lake is designated as "type II". Furthermore, "type IIa" depressions and lakes signify correct matches in both locations and shapes, while "type IIb" features only signify location matches because the area of any given lake should not exceed that of its host depression.

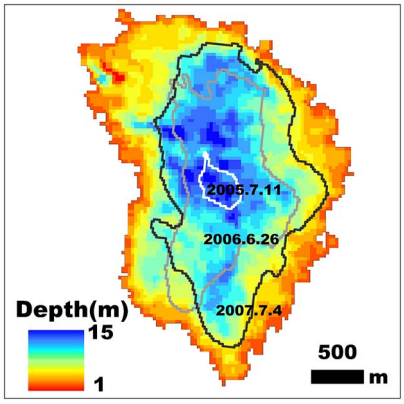

Fig. 4. Example of type IIa depression and lake. The type IIa depression is larger than its maximum corresponding lake detected from the satellite images. For this type IIa depression, lakes on three dates are detected and the one on July 4, 2007 (black line) is the largest one and labeled as type IIa lake.

filled or nearly filled with water when the satellite images used to generate the DEM were acquired. Such features were designated as type I lakes.

2) A DEM depression with no observed lake, resulting from either DEM noise or moulin development within a true topographic catchment, thus preventing accumulation of water (a third possibility, i.e., that the depression was real but its catchment was too cold to melt was unlikely here as the satellite images were examined below ELA during summer). Such features were defined as type I depressions.
3) A spatially coincident DEM depression and observed lake, signifying that the DEM dataset correctly detected true topographic depression on the ice sheet surface. These depressions associated with lake(s) were designated as type II lakes and depressions, respectively. A further refinement to type II features was made as follows. The area of any given lake should not exceed that of its host depression, so type II depressions with areas matching or exceeding the total area of its corresponding lake(s) were assumed to be correct ice sheet topography. Such features were designated type IIa depressions and lakes, respectively (Fig. 4). If the area of a depression was smaller than that of its corresponding lake, the DEM was assumed to correctly identify a lake's location but not the shape of its host depression. Such features were defined as type IIb depressions and lakes, respectively.

Note that real-world temporal changes between the timings of DEM and satellite image capture (e.g., lake catchment expansion) could also lead to type IIb designations. Barring such temporal changes, a comparison and summarization of type I, type II, and type IIa/IIb depressions and lakes enables an independent assessment of the capacity of moderate resolution DEMs for locating sinks for meltwater runoff generated on the ice sheet surface.

F. Comparison of DEM-Modeled Drainage Networks With Remotely Sensed Supraglacial Rivers

Modeling terrestrial drainage networks from DEM data has been studied for decades [15]. This study adopted a standard DEM-based hydrologic analysis approach (i.e., the D8 algorithm) that was implemented in ArcGIS software [40]. First, all the depressions in DEM data were fully filled (100% DEM filling). Second, the flow direction was identified and downstream flow accumulation grids calculated. Third, an accumulation threshold was selected to create drainage networks. A larger threshold reduced the number of extracted networks, avoiding redundant or artificial networks, whereas a smaller threshold created additional networks, of which many were spurious [18]. Because the drainage pattern of the actively flowing supraglacial river networks varied over space and time, it was necessary to empirically determine an accumulation area threshold [2]. For the WV2 mapping period in this study (July 18–23, 2012), the optimal accumulation area threshold was determined to be 500 pixels ($\sim$0.45 km^2), through a qualitative comparison between the modeled and mapped drainage networks to achieve a visually good match. To do this, two standard criteria were used, namely that locations of the modeled drainage heads should be roughly equivalent to the mapped rivers, and the length of the modeled drainage networks should be comparable to those of the mapped river networks [41]. Drainage networks derived from the SPIRIT DEM were used to carry out this comparison, and the resultant threshold then applied also to the GDEM to allow a uniform comparison between the two DEMs.

Comparison of DEM-modeled and observed drainage patterns is commonly achieved in terrestrial systems using visual qualitative assessments of those drainage networks and/or simple quantitative assessments of the hydrologic parameters (e.g., drainage area, flow path length, slope, and sinks filled) [16]–[18]. However, most of these assessments cannot provide measurable variables to directly depict the differences between different drainage networks. Therefore, a more fundamental approach capable of quantitatively assessing differences between the modeled and observed drainage networks is required. We employed two quantitative accuracy metrics to compare the drainage networks modeled by the DEM data with the supraglacial river networks delineated from WV2 satellite images [42]. A nested sequence of buffers with increasing size is applied around both DEM-modeled and observed drainage patterns. The similarity of these two drainage patterns is illustrated by plotting the statistical results for different

TABLE I
SUMMARY STATISTICS OF TOPOGRAPHIC DEPRESSIONS AND SUPRAGLACIAL LAKES

		Depression	Depression I	Depression II			Lake	Lake I	Lake II		
				II	IIa	IIb			II	IIa	IIb
Number	SPIRIT	14 000	11 625	2375	993	1382	2311	504	1807	1099	708
	GDEM	81 280	76 466	4814	1348	3466		154	2157	1430	727
Area (km^2)	SPIRIT	1563	506	1057	823	234	710	23	687	355	332
	GDEM	3558	2369	1189	854	335		4	706	343	363
Average Area (km^2)	SPIRIT	0.11	0.04	0.45	0.83	0.17	0.31	0.05	0.38	0.32	0.47
	GDEM	0.04	0.03	0.25	0.63	0.10		0.03	0.33	0.24	0.50

buffer widths. First, we calculated completeness, i.e., the total length of mapped rivers inside the buffered DEM modeled ones divided by total mapped river length. Second, we calculated miscoding, i.e., the length of DEM modeled rivers outside the buffered mapped ones divided by total modeled river length. Broad-scale comparison was achieved via large buffer sizes, while narrow-scale comparison via small buffer sizes represented the similarity between modeled and mapped planform in details.

IV. RESULTS

A. Ability of DEMs to Predict Supraglacial Lake Locations

In total, 14 000 (81 280) depressions ($A_{dep} = 0.01$ km^2) were extracted from SPIRIT DEM (GDEM) with a total area of 1563 (3558) km^2 covering 6.5% (14.9%) of the study area (Table I). Only 17.0% and 5.9% of these depressions from SPIRIT DEM and GDEM, respectively, were type II, indicating the vast majority of depressions extracted from both DEMs did not contain pooled water and were likely noise. Furthermore, type IIa depressions comprised only 7.1% for SPIRIT DEM and 1.7% for GDEM, indicating a generally poor match between DEM depressions and observed supraglacial lakes on the ice sheet. Additionally, the GDEM yielded more artificial depressions than the SPIRIT DEM.

From the perspective of supraglacial lakes, 1807 and 2157 type II lakes were identified by SPIRIT DEM an d GDEM, accounting for 78.2% and 93.3% of the total supraglacial lakes, respectively, whereas the corresponding percentages of type IIa lakes decreased to 47.6% and 61.9%, respectively. This result demonstrated that both DEMs successfully identified the locations of majority of actual supraglacial lakes (>75% identified), while they both lacked the ability (<62% identified) to reproduce those lakes realistically (depression areas should be larger than their associated lake areas). In addition, type IIb lake areas (A) exceeded their corresponding depression areas by large margins, which were larger by a factor of 2.2 ± 1.1 and 2.4 ± 1.1 for SPIRIT DEM and GDEM, respectively. If all the lakes/depressions are conical and have a constant diameter-depth ratio (α) [25], [43], the resultant volume ($V = (2\alpha/3\sqrt{\pi})\, A^{3/2}$) will be larger by a factor of 3.3 ± 1.2 and 3.7 ± 1.2 for SPIRIT DEM and GDEM, respectively.

In addition, the areas of the depressions/supraglacial lakes varied significantly among different depression/lake types. For instance, average areas of type IIa depressions extracted from SPIRIT DEM and from GDEM were 0.83 km^2 and 0.63 km^2, respectively, much larger than the average areas extracted for type I depressions, which were 0.04 km^2 and 0.03 km^2, respectively. This observation illustrated that larger depressions were more likely depicting actual ice sheet surface topography rather than DEM noise. The supraglacial lake analysis showed similar results: the average areas of the type II supraglacial lakes were 0.32 km^2 for SPIRIT DEM and 0.24 km^2 for GDEM, much larger than those of type I supraglacial lakes, which were 0.05 km^2 and 0.03 km^2, respectively. This observation illustrated that both DEMs failed to capture smaller supraglacial lakes, but did fairly well at predicting the locations of larger lakes.

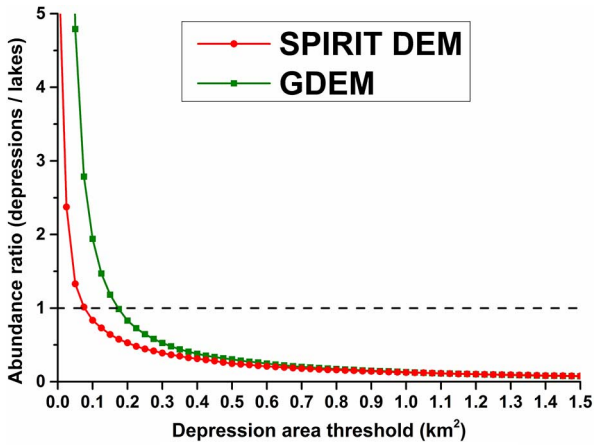

Fig. 5. Ratio of DEM-modeled depression abundance and remotely sensed supraglacial lake abundance under different depression area thresholds (A_{dep}) for the full study area (~24 000 km^2). At the scale of full study area, setting A_{dep} to 0.075 km^2 and 0.175 km^2 for SPIRIT DEM and GDEM, respectively, produces approximately equal counts of modeled and observed lakes.

B. Impacts of Depression Area Thresholds on DEM-Modeled Supraglacial Hydrology

Realism of DEM-modeled supraglacial hydrology was found to be critically sensitive to selection of the user-defined depression area threshold (A_{dep}). Specifically, comparisons of DEM-modeled depressions derived using different A_{dep} values with remotely sensed supraglacial lakes revealed that:

1) *Large A_{dep} values under-predicted supraglacial lake abundance while small A_{dep} values over-predicted abundance*. This finding is clearly revealed by plotting the ratio of modeled to observed lake abundance (Fig. 5). For example, setting $A_{dep} = 0.01$ km^2 over-predicted

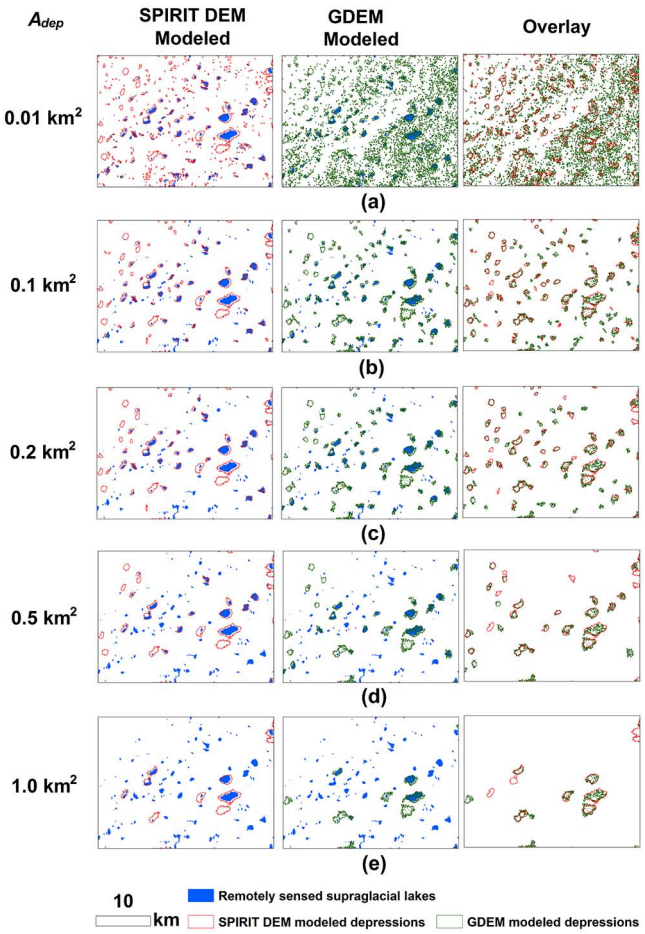

Fig. 6. Comparison of remotely sensed supraglacial lakes and DEM-modeled topographic depressions under different depression area thresholds (A_{dep}) for the red box region in Fig. 2. Small A_{dep} over-predicts lake abundance while large A_{dep} under-predicts abundance. (a) 0.01 km^2. (b) 0.1 km^2. (c) 0.2 km^2. (d) 0.5 km^2. (e) 1.0 km^2.

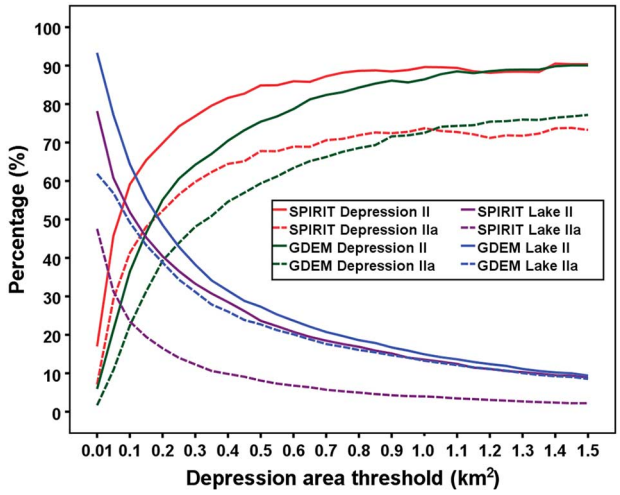

Fig. 7. Percentages of type II(a) DEM-modeled depressions in total depressions and percentages of type II(a) remotely sensed supraglacial lakes in total lakes under different depression area thresholds (A_{dep}). Larger depression percentages indicate better performances of A_{dep} to eliminate artificial depressions, whereas larger lake percentages indicate better performances of A_{dep} to reproduce observed lakes.

supraglacial lake abundance for 6.1 and 35.2 times for SPIRIT DEM and GDEM respectively, indicating that numerous artificial small depressions were obtained. Visual inspection of Fig. 6(a) illustrates this overestimation of lake abundance, with numerous artificial depressions not associated with observed lakes. In contrast, increasing A_{dep} created fewer depressions and lowered the lake abundance ratio (Fig. 5), leading to under-prediction of supraglacial lake abundance if A_{dep} was set too large. For example, the abundance ratio decreased to 0.1 for both DEMs when $A_{dep} = 1.5$ km^2, indicating that both DEMs failed to reproduce 90% of observed lakes at this setting. For this particular study area, setting A_{dep} to 0.075 km^2 and 0.175 km^2 for SPIRIT DEM and GDEM respectively generated the best overall match in total number of modeled and observed supraglacial lakes.

2) *Large A_{dep} values excluded more artificial depressions and vice versa.* The percentages of type II(a) depressions in total depressions were employed here as indicators (Fig. 7). When $A_{dep}>1$ km^2, both DEMs performed well to discern actual depressions from artificial ones: 73.7% of the obtained depressions were identified as type IIa depressions and 89.6% as type II depressions for SPIRIT DEM; these numbers were 72.5% and 86.4% for GDEM. Visual inspection in Fig. 6(e) further confirmed this result. Most of the large depressions had their associated lakes. However, these percentages decreased significantly with decreasing A_{dep} values. In addition, SPIRIT DEM performed better than GDEM to discern true depressions from artifacts when $A_{dep}<1$ km^2, whereas both DEMs performed similarly when $A_{dep}>1$ km^2.

3) *Larger A_{dep} values failed to identify more true depressions and vice versa.* The percentages of type II(a) supraglacial lakes in total lakes were employed as indicators (Fig. 7). When $A_{dep}>1$ km^2, both DEMs performed poorly in detecting supraglacial lakes [Fig. 6(a)]. The percentages of the identified type IIa and II supraglacial lakes were only 4.0% and 13.5% for SPIRIT DEM, and 13.2% and 14.9% for GDEM, respectively. However, these percentages increased substantially with decreased A_{dep} value. When $A_{dep} = 0.1$ km^2, $>55\%$ of the mapped lakes had their associated depressions (Fig. 7). Visual inspection in Fig. 6(b) further confirmed this result. In addition, GDEM performed better than SPIRIT DEM to identify true depressions.

4) *Selection of optimal A_{dep} values.* The optimal A_{dep} setting should reasonably reproduce the observed abundance of supraglacial lakes and achieve a good balance between artificial depression elimination and true depression identification. For this particular study area, 0.1 km^2 was determined to be the optimal A_{dep} value for SPIRIT DEM, and 0.2 km^2 for GDEM. By applying these two thresholds, the abundance ratios between modeled depressions and observed lakes were $\sim$0.85 (Fig. 5); moreover, the number percentages of type II depressions and lakes both exceeded 50% (i.e., 59% and 52% for SPIRIT DEM, and 52% and 50% for GDEM, see Fig. 7).

TABLE II
SUMMARY STATISTICS OF DIFFERENT TYPES OF MOULINS

		Moulin	Moulin I	Moulin II	Depression I	Depression II		
						II	IIa	IIb
Moulin number	SPIRIT	424	299	125	20	105	87	18
	GDEM		274	150	57	93	71	22
Percentage	SPIRIT	–	70.5%	29.5%	4.7%	24.8%	20.5%	4.3%
	GDEM		64.6%	35.4%	13.4%	21.9%	16.7%	5.2%

Type I moulin cannot be detected by using DEM data, whereas Type II moulin are distributed inside topographic depressions and thereby can be detected by using DEM data.

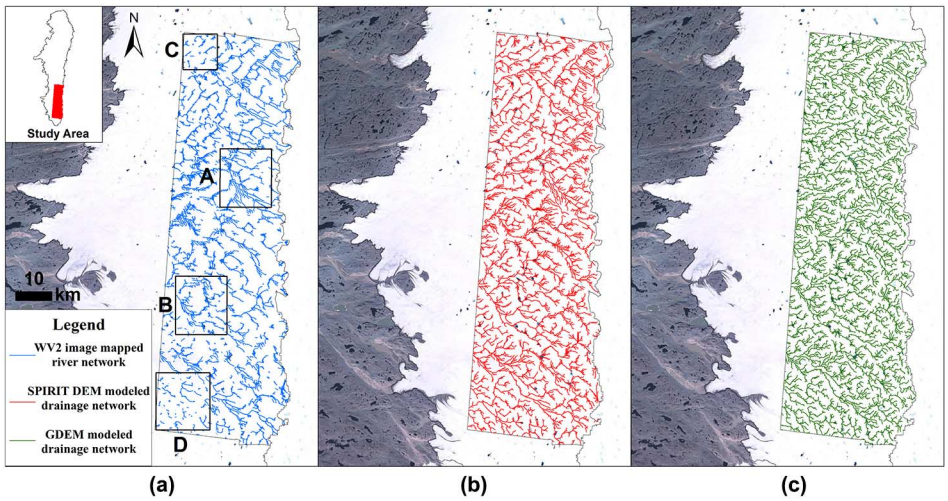

Fig. 8. Mapped and DEM-modeled supraglacial drainage networks. (a) Mapped river networks delineated from 21 WorldView-2 images acquired in July 2012. Drainage networks modeled by (b) SPIRIT DEM and (c) GDEM using the hydrologic analysis in ArcGIS software. A qualitatively derived accumulative area threshold (500 pixels, 0.45 km^2) is applied to generate the DEM-modeled drainage networks.

A visual inspection of depressions and lakes in Fig. 6(b) and (c) further supports the good performance of these two optimal thresholds. At these setting, the total abundances of depressions and lakes were comparable, and a majority of the DEM-modeled depressions were observed to contain supraglacial lakes in Landsat-7 and/or ASTER satellite imagery.

C. Ability of DEMs to Predict Moulin Locations

Moulins notably fragmented the mapped drainage networks and led to substantial differences between the terminations of the mapped and the modeled drainage networks. A total of 424 moulins were delineated from the high-resolution satellite images, with statistical results shown in Table II. Among these moulins, 299 were identified as type I moulins and were distributed outside of depressions ($A_{dep} = 0.01$ km^2) derived from SPIRIT DEM, accounting for 70.5% of the total moulin number; similarly, 274 moulins were denoted as type I using GDEM, accounting for 64.6% of the total number. This result showed that the majority of the moulin-based meltwater sinks ($>64\%$) on the ice surface were not identified by moderate-resolution DEMs.

Of the 125 type II moulins identified for SPIRIT DEM, 20 moulins (i.e., 16.0%) were located within type I depressions. For GDEM, the corresponding numbers were 150 and 57 (i.e., 38.0%), respectively (Table II). This result indicated that a portion of moulins developed in topographic depressions very early and had long survival times, leading to no lakes recorded in these depressions during 2000–2011. But some type I depressions were DEM noise, which occasionally contained moulins and also contributed to the derived percentages. Nevertheless, the above percentages offered upper boundaries to demonstrate the existences of that type of moulins.

D. Assessment of DEM-Modeled Drainage Networks

The total lengths of the modeled drainage networks were 4,018 km for SPIRIT DEM and 4,492 km for GDEM, which were 19.8% and 16.9% shorter, respectively, than that of the mapped river networks. This result was predictable because the spatial resolution of the WV2 multispectral images was 15 times higher than that of the DEM resolution and thus WV2 data showed more systematic details.

Both DEM-modeled drainage networks reasonably depicted the broad-scale drainage pattern of the trunk channels but not the low-order channels (Fig. 8). Regional differences could be observed in four subregions (regions A–D in Fig. 9). For region A and B, both DEMs identified the overall pattern of the main rivers but failed to depict the details of the drainage networks accurately. The drainage networks inferred from the SPIRIT DEM appeared to be more realistic than those from GDEM (see the black circles in Fig. 9). The differences were notably large for region C and D, both of which were located

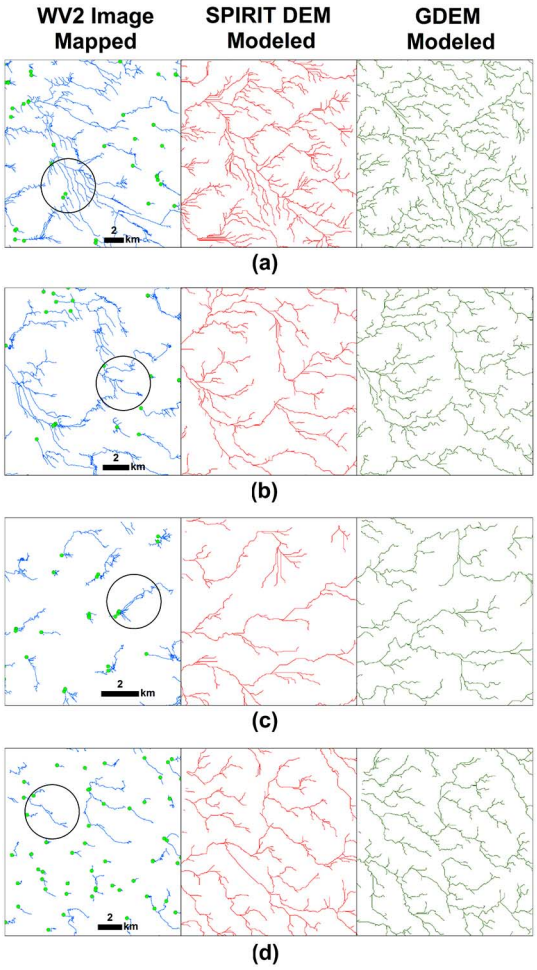

Fig. 9. Zoom-in images for region A–D [(a)–(d)] in Fig. 8. Moulins are shown in green points. Both DEMs generate surface drainage networks that are better continuous and less fragmented than reality owing to their poor ability to detect moulins. Black circles show the subregions where SPIRIT DEM performed better to model drainage pattern than GDEM.

near the outlet glacier and were consequently distributed among numerous crevasses, forming large number of type I moulins.

In addition, the drainage network comparison further supported the visual inspection that the DEM-modeled drainage networks matched well with the broad-scale drainage pattern of the mapped rivers, whereas they lacked the ability to match with the details of the mapped rivers (Fig. 10). For example, when the buffer size for drainage network comparison was 600 m (20 pixels), the completeness was 89.8% for SPIRIT DEM and 85.7% for GDEM, whereas the miscoding was only 25.0% for SPIRIT DEM and 37.6% for GDEM, respectively. This demonstrated that the tested DEMs reproduced $>85\%$ of the mapped river networks (completeness), while $<40\%$ of the modeled drainage pathways were artificial noise and did not match with any mapped rivers (miscoding) at a broad scale. However, when viewing from a much narrower scale, e.g., setting a buffer size of 90 m (3 pixels), the resultant completeness was $<30\%$, while miscoding was $>75\%$ for both DEMs. Quantitative analyses of completeness and miscoding revealed that the modeled drainage networks fairly represented the overall patterns of the mapped networks at broad scales (i.e., large buffer sizes) well, whereas yielding large positional offsets with the mapped river networks in details (i.e. small buffer sizes).

Finally, 100% filling of all depressions caused both DEMs to generate surface drainage networks that were more integrated and less fragmented than reality. In contrast, the mapped river networks were fragmented, mainly owing to the capture of supraglacial rivers by moulins (Figs. 8 and 9). This poor representation of DEM-modeled drainage networks was most significant at lower elevations (e.g., region C and D in Fig. 9), where numerous moulins form and the observed river networks are correspondingly short and fragmented. This result raises into question a standard practice of filling all DEM depressions for drainage pattern modeling on the GrIS surface.

V. Discussion

A. *Supraglacial Lake Area Implications*

While most of the supraglacial lake mapped in this study are small (i.e., $>70\%$ supraglacial lakes are smaller than 0.25 km^2) and thus cannot be confidently reproduced from the moderate resolution DEMs examined here, this does not negate the value of moderate-resolution DEMs for identifying important sinks for meltwater on the GrIS surface. Despite their abundance, the summed area of these small lakes is only 124 km^2, or 17% of the total mapped lake area. In addition, these small lakes are smaller than 4 pixels in MODIS imagery (spatial resolution is 250 m, commonly used in supraglacial lake studies) and thus cannot be confidently detected in MODIS images [25], [27]. Furthermore, the topographic depressions that host these small lakes generally have small volumes [25], [43], and unless a moulin develops, are likely to become fully filled and become meltwater flow paths soon after the melt season starts [13]. As such, a straightforward conclusion is that only the larger supraglacial lakes, as well as moulins, serve as significant terminal points for meltwater storage and fluxes on the ice sheet. Therefore, despite the low numeric correlations between modeled and observed supraglacial lakes (Table I), the moderate resolution DEMs examined here remain valuable for modeling the large topographic depressions of main importance for the storage of surface water on the ice surface.

To illustrate this, Fig. 11 presents the percentages of type II(a) supraglacial lakes (area >0.25 km^2) for the SPIRIT DEM and GDEM. Both DEMs exhibit significantly improved abilities to detect these large supraglacial lakes, with little difference between the two datasets. For instance, if the optimal thresholds (i.e., $A_{dep} = 0.1$ km^2 for SPIRIT DEM and 0.2 km^2 for GDEM) were applied, the resultant depressions successfully predicted the presence of supraglacial lakes 91% and 86% of the study region, respectively. Therefore, both DEMs perform quite well in detecting the most important storages of surface meltwater.

B. *Moulin Implications*

Moulins significantly fragment the supraglacial drainage pattern and thus play an important role in supraglacial drainage pattern formation and dynamics. However, it is quite difficult

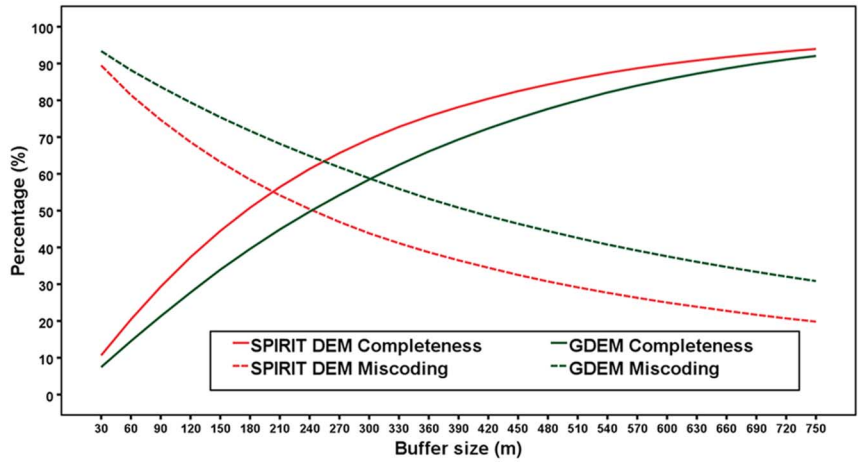

Fig. 10. Completeness and miscoding for the SPIRIT DEM and GDEM modeled drainage networks relative to the remotely sensed supraglacial river networks. Higher completeness and lower miscoding values show better matches between DEM-modeled and remotely sensed drainage networks.

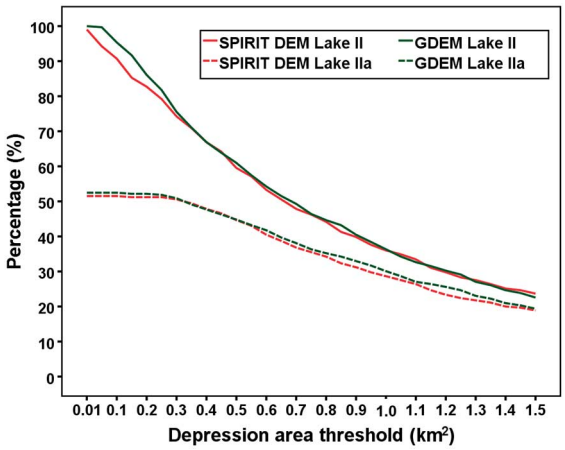

Fig. 11. Percentages of supraglacial type II(a) lake (>0.25 km^2) in total observed lakes for SPIRIT DEM and GDEM. Compared with the lake percentage curves in Fig. 7, both DEMs exhibit significantly improved abilities to detect large lakes, with little difference between the two products.

to identify moulins due to their small sizes, so knowledge of their spatial distribution, temporal evolution, and mechanism is lacking [44]. This study suggests that the majority of the extracted moulins ($\sim$70%) form at the intersections of rivers and crevasses (type I moulin), not at the bottom of supraglacial lakes (type II moulin). This challenges the prospect of simulating GrIS moulin distribution over large areas of the ice sheet using moderate resolution DEMs, since only type II moulins are associated with large depressions that are easily discerned in such products. This finding revealed the complex mechanism of moulin formation and further confirmed the conclusion in [2] that DEM data alone cannot fully describe supraglacial drainage and its connection to subglacial systems.

Depression area provides some useful clues to identify type II moulins. Based on the SPIRIT DEM, the average depression area to host such moulins is 1.2 ± 1.3 km^2, much larger than the average depression area (0.1 ± 0.3 km^2). For GDEM, the corresponding averages are 0.8 ± 1.0 km^2 (and 0.1 ± 0.1 km^2), respectively. This suggests that type II moulins are more likely to form inside large depressions. While no evidence was found to support a unifying critical area- or depth-dependent lake drainage threshold hypothesis, further analysis of the relationships between depression area and lake drainage may provide additional testing of this idea.

C. Drainage Network Comparison Implications

A clear conclusion of this study is that the DEM-modeled drainage networks can depict the overall shape of the mapped networks, but they do not match with the mapped river networks in details. However, certain limitations exist in this analysis that should be further analyzed. To what extent such limitations are due to DEM resolution and/or inaccuracies, or temporal changes in the river course positions themselves is unknown. While generally stable over time [45], supraglacial river networks do undergo morphological changes throughout the melt season [9], leading to considerable variations in location and reflectance properties of water-filled melt channels and consequently, impair this assessment of DEM accuracy. These river course changes can be attributed to the varied horizontal motion, vertical melting, and meltwater supply (influencing hydraulic geometry) on the ice sheet surface. This temporal evolution may also occur to supraglacial lakes: lake catchments may expand over time, inducing lakes larger than their corresponding DEM-modeled depressions. Barring the impacts of data sources and processing procedures [29], [30], the better performance of SPIRIT DEM over GDEM in modeling drainage networks partially implies the effects of river changes over time. Specifically, the SPOT5 images used to construct SPIRIT DEM were acquired after 2007, whereas the ASTER images used to construct GDEM were acquired after 2000, the majority of which were acquired before 2007. However, this conclusion needs further investigation by using newly released GrIS DEMs, such as the stereo-photogrammetric DEMs generated by WorldView-1/2 images obtained after 2011 [46].

Moreover, it is crucial to verify that DEMs are not over-filled in drainage network modeling (see Section III-F). Specifically,

river channels or large-scale topographic undulations may also be filled besides topographic depressions in DEM-filling processing. However, these situations do not occur for the GrIS DEMs: first, the GrIS elevation decreases from inland to ice margin so there are not large scale topographic undulations; and second, supraglacial river channels are generally too narrow to be identified in the moderate-resolution DEMs [10]. Therefore, all the depressions filled are small surface lows or DEM noise. This is supported by the sizes and shapes of the modeled depressions ($\sim 0.04-0.11$ km^2, see Table I and Fig. 6), and by the dendritic pattern of the modeled drainage networks (see Figs. 8 and 9; if the DEMs are over-filled/over-smoothed, there will be very long parallel drainage channels).

Importantly, the moderate-resolution DEMs examined here fail to reproduce the fragmentary natures of supraglacial river networks because they cannot predict most of the remotely sensed moulins. This suggests that the common practice of filling all DEM depressions in hydrologic analysis is problematic to apply on the ice surface. A similar finding has been reported in the prairie region of Canada [22]. The 100% DEM filling approach significantly overestimated the connectivity of drainage networks on the ice sheet and ignored the internally meltwater draining process. In reality, numerous supraglacial river networks of varying sizes form and efficiently drain meltwater into ice sheet through moulins [2], [20]. Without knowledge of drainage network fragmentation and meltwater sinks, it is difficult to answer some key questions, such as where and how much meltwater flows into the ice sheet, by using DEM data alone. Consequently, the continuous drainage networks modeled by DEMs may overestimate the runoff that leaves the ice sheet. More efforts are required to drive DEMs to model the fragmented drainage networks and meltwater sinks (i.e., moulins), which are more similar to the observed hydrologic pattern. We suggest that the following two approaches can mitigate this problem. First, more precise depression area thresholds and higher resolution DEMs (e.g., 2 m WorldView-1/2 DEM [46]) both can acquire more actual topographic depressions and thus identify more meltwater sinks. Second, the long residence time of some moulins (e.g., $\sim$11 years [47]) may facilitate moulin identification, as these stable moulins can be used as stable meltwater sinks in the DEM-based supraglacial hydrologic modeling.

Finally, questions exist with respect to the fact that the accumulation area threshold is arbitrarily selected in this study. Although this threshold is selected based on qualitative assessments, it still may result in drainage networks that are over-extracted or under-extracted [41]. Many attempts have been made to automatically calculate a suitable accumulation area threshold for terrestrial DEMs, but most of these require human intervention and thus are semiautomatic approaches [48]. Furthermore, this "optimal" threshold may not exist for the entire study area due to the local variability of topographical characteristics, and locally tuned thresholds may perform better [18], [41]. For the ice surface, a basic assumption is that the optimal thresholds may vary in space and time due to the large variations in surface topography and meltwater production, while a general relationship (or even an equation) among accumulation thresholds, elevation, runoff, temperature, albedo, and river width can be expected after a localized comparison between DEM-modeled and satellite-observed supraglacial drainage networks.

VI. Conclusion

One of the least understood hydrologic systems on Earth is the transport and release of meltwater on the GrIS surface. DEMs offer potential for application to GrIS supraglacial hydrologic analysis, but their suitability for this purpose has received little quantitative assessment. In this study, we compared remotely sensed supraglacial hydrologic features (lakes, rivers, and moulins) against the ability of two moderate-resolution GrIS DEMs (SPIRIT DEM and ASTER GDEM) to reproduce these features. We suggest that realism of DEM-modeled supraglacial hydrology is critically sensitive to selection of depression area thresholds. Useful insight about the benefits and limitations of using moderate-resolution DEMs to model the flow of meltwater passing over and into the ice sheet surface was also provided. However, our results also indicate several areas for improvement. First, performance of depression area thresholds was evaluated over the whole study area. However, sizes and distributions of topographic depressions on the ice surface vary spatially; therefore, future work should develop adaptive thresholds. Second, the results in this paper should be expanded and linked to larger scale hydrologic modeling (e.g., watershed scale) on the ice sheet to illustrate the impacts of meltwater transport and release on the ice sheet mass balance. Third, the hydrologic impact of DEM spatial resolution should be studied and the performance of higher-resolution DEMs (e.g., 2 m WorldView-1/2 DEMs) should be estimated. Despite these issues, our results show that users need to be aware of the critical sensitivity of depression area thresholds, avoid predicting moulin locations, and avoid 100% filling when using DEMs to represent the supraglacial hydrology of the Greenland Ice Sheet.

Acknowledgment

SPIRIT DEM data are courtesy of the CNES/Spot Image SPIRIT program. WorldView-2 imagery was provided by the Polar Geospatial Center, University of Minnesota, during a Visiting Studentship at UCLA. The authors thank the anonymous reviewers for their detailed and constructive comments on this paper.

References

[1] M. Van den Broeke *et al.*, "Partitioning recent Greenland mass loss," *Science*, vol. 326, no. 5955, pp. 984–986, 2009.

[2] L. C. Smith *et al.*, "Efficient meltwater drainage through supraglacial streams and rivers on the southwest Greenland ice sheet," *Proc. Natl. Acad. Sci. USA*, vol. 112, no. 4, pp. 1001–1006, 2015.

[3] E. M. Enderlin *et al.*, "An improved mass budget for the Greenland ice sheet," *Geophys. Res. Lett.*, vol. 41, pp. 866–872, 2014.

[4] J. Ettema *et al.*, "Higher surface mass balance of the Greenland ice sheet revealed by high-resolution climate modeling," *Geophys. Res. Lett.*, vol. 36, no. 12, p. L12501, 2009.

[5] I. M. Howat *et al.*, "Rates of southeast Greenland ice volume loss from combined ICESat and ASTER observations," *Geophys. Res. Lett.*, vol. 35, no. 17, p. L17505, 2008.

[6] V. W. Chu, "Greenland ice sheet hydrology: A review," *Prog. Phys. Geogr.*, vol. 38, no. 1, pp. 19–54, 2013.

[7] D. McGrath *et al.*, "Assessing the summer water budget of a moulin basin in the Sermeq Avannarleq ablation region, Greenland ice sheet," *J. Glaciol.*, vol. 57, no. 205, pp. 954–964, 2011.

[8] I. Joughin *et al.*, "Influence of ice-sheet geometry and supraglacial lakes on seasonal ice-flow variability," *Cryosphere*, vol. 7, no. 4, pp. 1185–1192, 2013.

[9] D. J. Lampkin and J. VanderBerg, "Supraglacial melt channel networks in the Jakobshavn Isbræ region during the 2007 melt season," *Hydrol. Process.*, vol. 28, no. 25, pp. 6038–6053, 2014.

[10] K. Yang and L. C. Smith, "Supraglacial streams on the Greenland ice sheet delineated from combined spectral-shape information in high-resolution satellite imagery," *IEEE Geosci. Remote Sens. Lett.*, vol. 10, no. 4, pp. 801–805, Jul. 2013.

[11] A. F. Banwell *et al.*, "Modeling supraglacial water routing and lake filling on the Greenland ice sheet," *J. Geophys. Res.*, vol. 117, no. F4, p. F04012, 2012.

[12] A. A. Leeson *et al.*, "Simulating the growth of supraglacial lakes at the western margin of the Greenland ice sheet," *Cryosphere*, vol. 6, no. 5, pp. 1077–1086, 2012.

[13] N. S. Arnold, A. F. Banwell, and I. C. Willis, "High-resolution modelling of the seasonal evolution of surface water storage on the Greenland Ice Sheet," *Cryosphere*, vol. 8, no. 4, pp. 1149–1160, 2014.

[14] C. C. Clason *et al.*, "Modelling the transfer of supraglacial meltwater to the bed of Leverett Glacier, Southwest Greenland," *Cryosphere*, vol. 9, no. 1, pp. 123–138, 2015.

[15] J. Fairfield and P. Leymarie, "Drainage networks from grid digital elevation models," *Water Resour. Res.*, vol. 27, no. 5, pp. 709–717, 1991.

[16] T. Kenward *et al.*, "Effects of digital elevation model accuracy on hydrologic predictions," *Remote Sens. Environ.*, vol. 74, no. 3, pp. 432–444, 2000.

[17] J. P. Walker and G. R. Willgoose, "On the effect of digital elevation model accuracy on hydrology and geomorphology," *Water Resour. Res.*, vol. 35, no. 7, pp. 2259–2268, 1999.

[18] J. Li and D. W. S. Wong, "Effects of DEM sources on hydrologic applications," *Comput. Environ. Urban Syst.*, vol. 34, no. 3, pp. 251–261, 2010.

[19] S. M. Lewis and L. C. Smith, "Hydrologic drainage of the Greenland Ice Sheet," *Hydrol. Process*, vol. 23, no. 14, pp. 2004–2011, 2009.

[20] K. Poinar *et al.*, "Limits to future expansion of surface-melt-enhanced ice flow into the interior of western Greenland," *Geophys. Res. Lett.*, vol. 42, no. 6, pp. 1800–1807, 2015.

[21] J. B. Lindsay and I. F. Creed, "Distinguishing actual and artefact depressions in digital elevation data," *Comput. Geosci.*, vol. 32, no. 8, pp. 1192–1204, 2006.

[22] S. Li *et al.*, "Lidar DEM error analyses and topographic depression identification in a hummocky landscape in the prairie region of Canada," *Geomorphology*, vol. 129, no. 3–4, pp. 263–275, 2011.

[23] A. A. W. Fitzpatrick *et al.*, "A decade of supraglacial lake volume estimates across a land-terminating margin of the Greenland Ice Sheet," *Cryosphere*, vol. 8, no. 1, pp. 107–121, 2014.

[24] N. Selmes, T. Murray, and T. D. James, "Fast draining lakes on the Greenland ice sheet," *Geophys. Res. Lett.*, vol. 38, no. 15, p. L15501, 2011.

[25] Y.-L. Liang *et al.*, "A decadal investigation of supraglacial lakes in West Greenland using a fully automatic detection and tracking algorithm," *Remote Sens. Environ.*, vol. 123, pp. 127–138, 2012.

[26] B. F. Morriss *et al.*, "A ten-year record of supraglacial lake evolution and rapid drainage in West Greenland using an automated processing algorithm for multispectral imagery," *Cryosphere*, vol. 7, no. 6, pp. 1869–1877, 2013.

[27] A. V. Sundal *et al.*, "Evolution of supra-glacial lakes across the Greenland Ice Sheet," *Remote Sens. Environ.*, vol. 113, no. 10, pp. 2164–2171, 2009.

[28] M. Tedesco *et al.*, "Ice dynamic response to two modes of surface lake drainage on the Greenland ice sheet," *Environ. Res. Lett.*, vol. 8, no. 3, p. 034007, 2013.

[29] J. Korona *et al.*, "SPIRIT. SPOT 5 stereoscopic survey of Polar Ice: Reference images and topographies during the fourth International Polar Year (2007–2009)," *ISPRS J. Photogramm. Remote Sens.*, vol. 64, no. 2, pp. 204–212, 2009.

[30] A. J. Cook *et al.*, "A new 100-m digital elevation model of the Antarctic Peninsula derived from ASTER Global DEM: Methods and accuracy assessment," *Earth Syst. Sci. Data*, vol. 4, no. 1, pp. 129–142, 2012.

[31] S. M. Hvidegaard, L. Sandberg Sørensen, and R. Forsberg, "ASTER GDEM validation using LiDAR data over coastal regions of Greenland," *Remote Sens. Lett.*, vol. 3, no. 1, pp. 85–91, 2011.

[32] I. M. Howat, A. Negrete, and B. E. Smith, "The Greenland Ice Mapping Project (GIMP) land classification and surface elevation data sets," *Cryosphere*, vol. 8, no. 4, pp. 1509–1518, 2014.

[33] C. J. Tucker, D. M. Grant, and J. D. Dykstra, "NASA's global orthorectified Landsat data set," *Photogramm. Eng. Remote Sens.*, vol. 70, no. 3, pp. 313–322, 2004.

[34] S. V. Nghiem *et al.*, "The extreme melt across the Greenland ice sheet in 2012," *Geophys. Res. Lett.*, vol. 39, no. 20, p. L20502, 2012.

[35] J. Li and Y. Sheng, "An automated scheme for glacial lake dynamics mapping using Landsat imagery and digital elevation models: A case study in the Himalayas," *Int. J. Remote Sens.*, vol. 33, no. 16, pp. 5194–5213, 2012.

[36] N. Otsu, "A threshold selection method from gray-level histograms," *IEEE Trans. Syst. Man Cybern.*, vol. 9, no. 1, pp. 62–66, Jan. 1979.

[37] D. J. Lampkin and J. VanderBerg, "A preliminary investigation of the influence of basal and surface topography on supraglacial lake distribution near Jakobshavn Isbrae, western Greenland," *Hydrol. Process.*, vol. 25, no. 21, pp. 3347–3355, 2011.

[38] W. A. Sneed and G. S. Hamilton, "Evolution of melt pond volume on the surface of the Greenland Ice Sheet," *Geophys. Res. Lett.*, vol. 34, no. 3, p. L03501, 2007.

[39] N. Arnold, "A new approach for dealing with depressions in digital elevation models when calculating flow accumulation values," *Prog. Phys. Geogr.*, vol. 34, no. 6, pp. 781–809, 2010.

[40] S. K. Jenson and J. O. Domingue, "Extracting topographic structure from digital elevation data for geographic information-system analysis," *Photogramm. Eng. Remote Sens.*, vol. 54, no. 11, pp. 1593–1600, 1988.

[41] S. C. Mest, D. A. Crown, and W. Harbert, "Watershed modeling in the Tyrrhena Terra region of Mars," *J. Geophys. Res. Planets*, vol. 115, p. E09001, 2010.

[42] H. Tveite, "An accuracy assessment method for geographical line data sets based on buffering," *Int. J. Geogr. Inf. Sci.*, vol. 13, no. 1, pp. 27–47, 1999.

[43] M. J. Krawczynski *et al.*, "Constraints on the lake volume required for hydro-fracture through ice sheets," *Geophys. Res. Lett.*, vol. 36, no. 10, p. L10501, 2009.

[44] A. K. Rennermalm *et al.*, "Understanding Greenland ice sheet hydrology using an integrated multi-scale approach," *Environ. Res. Lett.*, vol. 8, no. 1, p. 015017, 2013.

[45] L. Karlstrom, P. Gajjar, and M. Manga, "Meander formation in supraglacial streams," *J. Geophys. Res. Earth Surf.*, vol. 118, no. 3, pp. 1897–1907, 2013.

[46] M.-J. Noh and I. M. Howat, "Automated stereo-photogrammetric DEM generation at high latitudes: Surface extraction with TIN-based search-space minimization (SETSM) validation and demonstration over glaciated regions," *GIsci Remote Sens.*, vol. 52, no. 2, pp. 198–217, 2015.

[47] G. A. Catania and T. A. Neumann, "Persistent englacial drainage features in the Greenland Ice Sheet," *Geophys. Res. Lett.*, vol. 37, no. 2, p. L02501, 2010.

[48] D. G. Tarboton, R. L. Bras, and I. Rodriguezіturbe, "On the extraction of channel networks from digital elevation data," *Hydrol. Process.*, vol. 5, no. 1, pp. 81–100, 1991.

Kang Yang received the Ph.D. degree in geography from Nanjing University, Nanjing, China, in 2014.

He is currently a Postdoctoral Scholar with the Department of Geography, University of California, Los Angeles, CA, USA. His research interests include Greenland ice sheet hydrology and river remote sensing.

Laurence C. Smith received the Ph.D. degree in earth and atmospheric sciences from Cornell University, Ithaca, NY, USA, in 1996.

He is currently a Professor and Chair of Geography, and a Professor of Earth, Planetary, and Space Sciences with the University of California, Los Angeles, CA, USA. He has authored over 80 peer-reviewed articles, essays, and books including *Science*, *Nature*, and *PNAS*. His research interests include the Arctic, hydrology, satellite remote sensing technologies, and climate change.

Prof. Smith was named a Guggenheim Fellow by the John S. Guggenheim Foundation in 2006–2007. In 2015, he was elected as the Fellow of the American Geophysical Union (AGU).

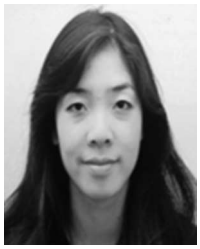

Vena W. Chu received the Ph.D. degree in geography from the University of California, Los Angeles, CA, USA, in 2015.

She is currently a University of California President's Postdoctoral Fellow with the Department of Geography, University of California, Berkeley, CA, USA. Her research interests include geospatial technologies and field observations to understand Arctic hydrologic systems.

Colin J. Gleason received the M.S. degree in geospatial engineering from the State University of New York College of Environmental Science and Forestry, Syracuse, NY, USA, in 2011.

He is currently a Doctoral Candidate with the Department of Geography, University of California, Los Angeles, CA, USA. His research interests include fluvial hydrology, geography, and remote sensing.

Manchun Li received the Ph.D. degree in cartography from Nanjing University, Nanjing, China, in 1992.

He is currently a Professor with the Department of Geographic Information Science, Nanjing University, China. He has authored over 50 peer-reviewed articles. His research interests include geographic information system and remote sensing applications.